One-pot synthesis of multifunctional iron- and manganese-loaded biochar from durian husks for photo-Fenton degradation of tartrazine

Hung Minh Nguyen[1,2], Tin Trung Nguyen[1,2], Tien Minh Van[1,2],
Tuyet-Mai Tran-Thuy[1,2], Long Quang Nguyen[1,2], Dung Van Nguyen[1,2]*

[1] Faculty of Chemical Engineering, Ho Chi Minh City University of Technology (HCMUT), 268 Ly Thuong Kiet Street, Dien Hong Ward, Ho Chi Minh City, Vietnam
[2] Vietnam National University Ho Chi Minh City, Linh Xuan Ward, Ho Chi Minh City, Vietnam
* Corresponding author's e-mail: nvdung@hcmut.edu.vn

ABSTRACT

The current research proposes a novel approach to fabricate multifunctional iron- and manganese-loaded biochar (FeMn/BC) through one-pot pyrolysis of $FeCl_3$- and $KMnO_4$-impregnated durian husks (DHs). Analytical results indicated the presence of 5.72 wt% Fe (Fe_3O_4 and Fe^0) and 2.90 wt% Mn (MnO) within the biochar (BC) matrix. Regarding porous properties, FeMn/BC possessed a specific surface area (S_{BET}) of 292 m²/g and a total pore volume (V_{total}) of 0.19 cm³/g. Accordingly, FeMn/BC was explored as a photo-Fenton catalyst for tartrazine (TZ) degradation. At pH 3.0, 200 ppm H_2O_2, and UV light, 0.50 g/L FeMn/BC treated 92.0% TZ (50 ppm) within 10 min of adsorption and 120 min of oxidation. In addition, FeMn/BC with a saturation magnetization (M_S) of 5.13 emu/g could be separated from treated mixtures by external magnetic fields. Overall, the multifunctional FeMn/BC prepared from DH waste demonstrated its magnetic separability and efficacy in treating TZ.

Keywords: durian husk, biomass valorization, multifunctional material, metal-loaded biochar, one-pot strategy, photo-Fenton, tartrazine.

INTRODUCTION

Water pollution resulting from organic contaminants has intensified recently, driven by the expansion of industrial, agricultural, and domestic activities (Wen et al., 2017). Organic pollutants, such as pesticides, dyes, surfactants, industrial solvents, and pharmaceutical residues, often have complex and stable molecular structures that make them resistant to conventional biological degradation processes (Intisar et al., 2023). Upon introduction into aquatic systems, these compounds deteriorate water quality and impose long-term ecotoxicological risks, even at trace concentrations, threatening both ecosystem integrity and human health (Li et al., 2024). In response to these challenges, Fenton and Fenton-like processes have emerged as promising advanced treatment methods for effectively removing such persistent organic pollutants from wastewater (Ahmed et al., 2025; Hardyanti et al., 2024). The classical Fenton reaction involves the interaction of ferrous ions (Fe^{2+}) with hydrogen peroxide (H_2O_2) to generate highly reactive hydroxyl radicals (•OH) that can degrade various organic contaminants. However, the homogeneous Fenton system typically generates substantial iron-containing sludge, making it less sustainable for large-scale or long-term applications (Cao et al., 2024). Hence, heterogeneous Fenton processes have been developed using solid iron-based catalysts such as Fe_3O_4, α-Fe_2O_3, γ-Fe_2O_3, α-FeOOH, and Fe^0 (Nguyen et al., 2024b; Zhu et al., 2019). These solid catalysts enhance the generation of hydroxyl radicals while simultaneously reducing iron leaching

and minimizing sludge formation (Ziembowicz and Kida, 2022). Moreover, heterogeneous systems enable more efficient catalyst recovery and reuse, thereby improving cost-effectiveness and environmental safety. The performance of these systems is further enhanced by the photo-Fenton technique, which employs UV irradiation to increase catalytic activity (Brillas, 2022; Rahim Pouran et al., 2015). Light facilitates the photoreduction of Fe^{3+} ions to Fe^{2+} ones, hence maintaining the redox cycle and enhancing the generation of hydroxyl radicals (Brillas and Garcia-Segura, 2020; O'Dowd and Pillai, 2020). This results in enhanced pollutant mineralization and diminished catalyst deactivation (Zhang et al., 2019).

Metal-based catalysts play a crucial role in enhancing the efficiency of Fenton and Fenton-like processes for wastewater treatment (Hussain et al., 2021). Iron-based catalysts are favored due to their abundance, low cost, environmental compatibility, and high efficiency in generating reactive radicals (Ribeiro et al., 2022). In addition to iron, other transition metals such as copper, silver, and manganese have also been employed to promote similar oxidative pathways, offering alternative catalytic activities and operational conditions (Liu and Wang, 2023). Among these metals, manganese can catalyze Fenton-like reactions, though it behaves differently from iron. Mn exists in multiple oxidation states (Mn^{2+}, Mn^{3+}, Mn^{4+}), enabling redox cycling that can decompose H_2O_2 and generate •OH radicals (Zheng et al., 2024). In bimetallic systems, the combination of iron and manganese has synergistic effects, as manganese facilitates the regeneration of Fe^{2+}, hence improving redox cycling (Chen et al., 2019; Li et al., 2019). Consequently, Fe–Mn binary oxides can boost catalytic activity for photo-Fenton processes (Li et al., 2021).

A major challenge in utilizing nano- or microscale metal particles is their tendency to agglomerate (Mekuye and Abera, 2023). Due to their high surface energy and strong intermolecular forces, metal particles readily aggregate, leading to reduced specific surface area, diminished active catalytic sites, and decreased reaction efficiency (Shrestha et al., 2020). Hence, an effective strategy is to immobilize metal particles onto supports, which improves their dispersion and prevents aggregation (Zhu and Xu, 2016). Among various potential supports, BC has garnered significant attention due to its exceptional properties (Faheem et al., 2020). Produced through the pyrolysis of

biomass under oxygen-limited conditions, BC typically possesses a porous structure, chemical stability, and abundant functional groups (Soffian et al., 2022). Additionally, BC is renewable, low-cost, and environmentally friendly, making it an attractive support for sustainable wastewater treatment (Yuan et al., 2023). To disperse metal particles onto the BC matrix, different approaches have been developed. Direct pyrolysis of metal salt-impregnated biomass not only immobilizes metals or their oxides on BC but also improves its porosity (Tran et al., 2024a; 2024b). For instance, Do et al. (2022) successfully incorporated Fe_3O_4 nanoparticles and nanowires into the BC matrix through one-pot pyrolysis of $FeCl_3$-impregnated lotus seed pods. The addition of $FeCl_3$ enhanced S_{BET} (349 m²/g) and V_{total} (0.31 cm³/g) of Fe_3O_4-loaded BC, markedly above the values of pristine BC (S_{BET} = 150 m²/g and V_{total} = 0.08 cm³/g). In another study, direct pyrolysis of $KMnO_4$-impregnated cotton stem produced MnO-loaded BC composite for efficient heavy metal removal from wastewater (Chang and Li, 2024). In this study, both $FeCl_3$ and $KMnO_4$ were impregnated in biomass for the first time, potentially producing iron and manganese oxides inside the BC matrix.

Durian (*Durio zibethinus*), is recognized as the "King of Fruits", which the remarkable tropical fruit grown and devoured locally in Southeast Asia countries like Malaysia, Indonesia, Thailand, the Philippines and Vietnam (Jamnongkan et al., 2022; Mohd Ali et al., 2020). Due to its strong aroma and unique taste, durian fruits enjoys high demand both locally and internationally. However, the consumption of durian fruits generates a large amount of waste, primarily from the husks – the thick, spiky outer shells (Lee et al., 2019; Nguyen et al., 2024a). These DHs are typically discarded as food waste without use. Improper disposal of DHs poses environmental challenges, including waste management issues and potential pollution. Hence, sustainable utilization of DHs is essential for waste reduction and economic value creation. In this research, we proposed a novel approach to valorize DHs into a multifunctional material. The DH biomass was first impregnated with $FeCl_3$ and $KMnO_4$, and the obtained mixture was pyrolyzed to yield FeMn/BC. The composite was used as a photo-Fenton catalyst to degrade tartrazine, a common food colorant with significant concerns regarding consumer safety (Amchova et al., 2024).

EXPERIMENTAL

Materials

DH residue was collected in Vinh Long Province, Vietnam. The biomass was washed with tap water and distilled water several times before being dried in an oven at 110 °C. DH was crushed finely and stored in a sealed container for further experiments. All chemicals were used directly without any refining process.

Preparation of FeMn/BC

First, 4.00 g of DH powder, 0.80 g of $FeCl_3$, and 0.40 g of $KMnO_4$ were mixed with distilled water for 18 h. The resulting mixture was then dried at 110 °C for 24 h and placed inside an oven. Pyrolysis was conducted at 600 °C for 1 h under a nitrogen flow rate of 250 mL/min. The solid product obtained was washed with distilled water to remove any water-soluble impurities, followed by drying again at 110 °C for 24 h to yield FeMn/BC. For comparison, biochar (BC), iron-loaded biochar (Fe/BC), and manganese-loaded biochar (Mn/BC) were prepared by pyrolyzing only DH, $FeCl_3$-impregnated DH, and $KMnO_4$-impregnated DH samples, respectively, using the same procedure.

Characterization of FeMn/BC

To characterize the crystalline phases present in FeMn/BC, powder X-ray diffraction (XRD) analysis was performed using a Bruker AXS D8 diffractometer with CuKα radiation (λ = 1.5418 Å) over a 2θ range of 10–80°. The Fe and Mn contents were quantified through acid digestion using concentrated HNO_3 at 60 °C for 1 h, followed by inductively coupled plasma optical emission spectrometry (ICP-OES) analysis using a Perkin Elmer Optima 7300DV instrument. S_{BET} and V_{total} (at P/P_0 = 0.992) were obtained from a Micromeritics Tristar II Plus analyzer. Magnetic properties of FeMn/BC were investigated using a vibrating-sample magnetometer (VSM) at room temperature. Fourier transform infrared (FTIR) spectroscopy was performed with a Tensor 27 spectrometer. Morphological characteristics were examined using scanning electron microscopy (SEM, JEOL JSM-IT200) and transmission electron microscopy (TEM, JEOL JEM-1010).

Tartrazine degradation using FeMn/BC

The catalytic activity of FeMn/BC was investigated through TZ degradation using H_2O_2 under UV light (Exo Terra Reptile UVB150 13 W) at 31 °C. First, 200 mL of TZ (50 ppm) and a certain catalyst dosage were added to a beaker. The mixture was stirred at a constant speed, and its initial pH value was adjusted by H_2SO_4 (0.5 M) and NaOH (0.1 M) solutions. After a 10-min adsorption period, a specific H_2O_2 dosage was introduced, and the UV lamp was simultaneously turned on for the photo-Fenton process. At designated time intervals, 2.0 mL samples were collected and immediately mixed with solutions containing $Na_2S_2O_3$ to neutralize excess H_2O_2 and phosphate buffer to maintain a pH of ≈7. Solid catalysts were separated from suspensions by centrifugation. TZ concentrations were then measured using a Jasco V-730 UV-Vis spectrophotometer. The TZ adsorption capacity and removal were calculated as follows:

$$\text{TZ adsorption capacity (mg/g)} = \frac{50 - C_0}{C_M} \quad (1)$$

$$\text{TZ removal (\%)} = \frac{50 - C_{120}}{50} \times 100\% \quad (2)$$

where: C_M (g/L) was the catalyst dosage, C_0 was the *TZ* concentration after 10 min of adsorption and the beginning of oxidation. C_{120} was the *TZ* concentration after 120 min of oxidation.

RESULTS AND DISCUSSION

Properties of FeMn/BC

The crystalline structure of FeMn/BC was determined by XRD (Figure 1). Although the BC matrix shows poor crystallinity, such crystals are found. The characteristic peaks at 2θ = 30.1, 35.5, 37.1, 43.1, 53.5, 57.0, and 62.6° correspond to the (220), (311), (222), (400), (422), (511), and (440) planes of Fe_3O_4 crystals, respectively (JCPDS Card No. 01-076-1849). In addition, the existence of Fe^0 crystals is evidenced by distinctive peaks at 2θ = 44.6 and 65.0° (JCPDS Card No. 06-0696). For the remaining metal, an overlapped peak at 2θ ≈ 35.5 and identified peaks at 2θ = 41.2 and 59.8° reveal the (111), (200), and (220) planes of MnO crystals, respectively (JCPDS Card No. 07-0230).
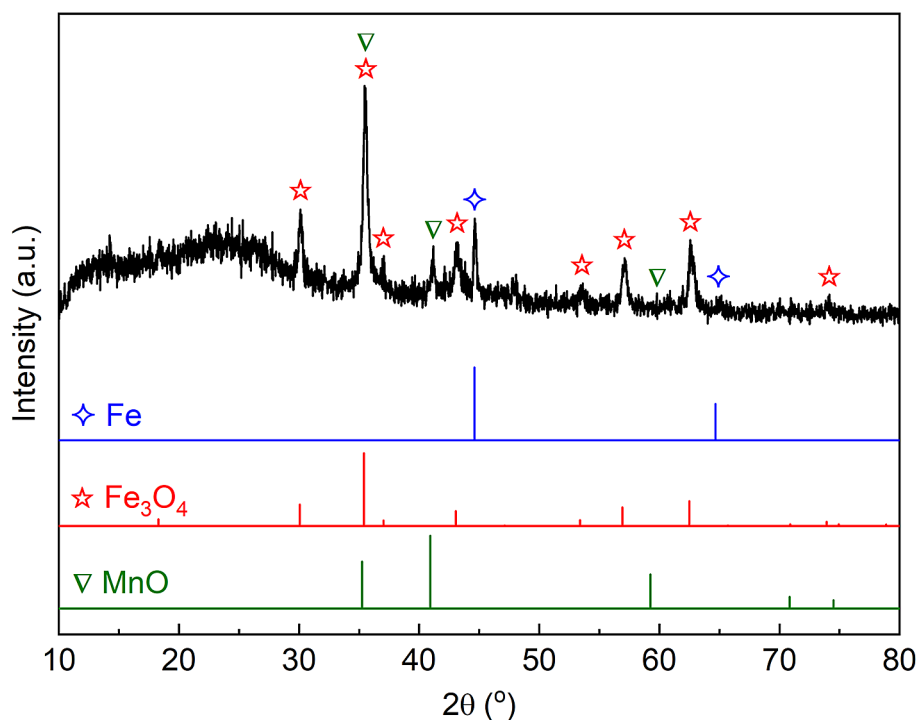
Figure 1. XRD pattern of FeMn/BC

Prior research indicates that pyrolysis of $FeCl_3$-impregnated biomass at 600 °C can potentially generate Fe_3O_4 and Fe^0 crystals embedded within the BC matrix (Nguyen et al., 2023a; 2023b). With $KMnO_4$-impregnated biomass, MnO is the final product (Chang and Li, 2024; Qiu et al., 2019). During those pyrolyses, carbon and certain gases formed from biomass carbonation can reduce metal salts and oxides into the aforementioned iron- and manganese-based crystals. With the utilization of both $FeCl_3$ and $KMnO_4$, other minor crystals might also be produced, or the identified crystals might be doped with the remaining metal. To summarize, Fe_3O_4 and Fe^0 were formed from $FeCl_3$, while MnO originated from $KMnO_4$. Moreover, ICP-OES results confirmed the presence of both Fe (5.72 wt%) and Mn (2.90 wt%) in FeMn/BC (Table 1).

Porous properties of BC, Fe/BC, Mn/BC, and FeMn/BC are detailed in Table 1. In the absence of metal salt additives, BC exhibits a relatively low S_{BET} of 45 m²/g and a very low V_{total} of 0.02 cm³/g. In contrast, Fe/BC shows a significantly enhanced S_{BET} of 283 m²/g and V_{total} of 0.24 cm³/g, indicating that $FeCl_3$ acted as an effective activating agent (Bedia et al., 2020). Similarly, $KMnO_4$ demonstrated activation potential, as Mn/BC achieves a S_{BET} of 240 m²/g and a V_{total} of 0.28 cm³/g. According to Qiu et al. (2019), during

$KMnO_4$-assisted biomass pyrolysis, the release of oxygen can etch the carbon surface, while the formation of K_2CO_3 further contributes to the development of porous structures. FeMn/BC prepared from both $FeCl_3$ and $KMnO_4$ has a high S_{BET} of 292 m²/g and a large V_{total} of 0.19 cm³/g. Compared to Fe/BC and Mn/BC, the simultaneous presence of metal-based phases in FeMn/BC did not significantly hinder the overall porosity.

The morphology of FeMn/BC was observed using SEM images (Figure 2). FeMn/BC exhibits irregular fragments with rough surfaces and structural distortions, likely resulting from mechanical grinding of DH biomass prior to carbonization. The observed grooves and cavities in these fragments directly correlate with the native structure of the raw material. These morphological features are consistent with those from a previous report of DH-derived carbon materials (Jamnongkan et al., 2022). The unique morphology of FeMn/BC might improve surface reactivity, interfacial interactions, and mass transfer, thereby facilitating its performance for environmental remediation.

The internal structure of FeMn/BC is illustrated using TEM images (Figure 3). The dark regions likely correspond to metal-based nanoparticles, as their higher atomic numbers lead to stronger electron scattering. In contrast, the lighter areas are likely associated with the BC matrix. Based on

Table 1. Properties of Fe/BC, Mn/BC and FeMn/BC

Sample	Fe (wt%)	Mn (wt%)	S_{BET} (m²/g)	V_{total} (cm³/g)
BC	-	-	45	0.02
Fe/BC	5.82	-	283	0.24
Mn/BC	-	4.26	240	0.28
FeMn/BC	5.72	2.90	292	0.19
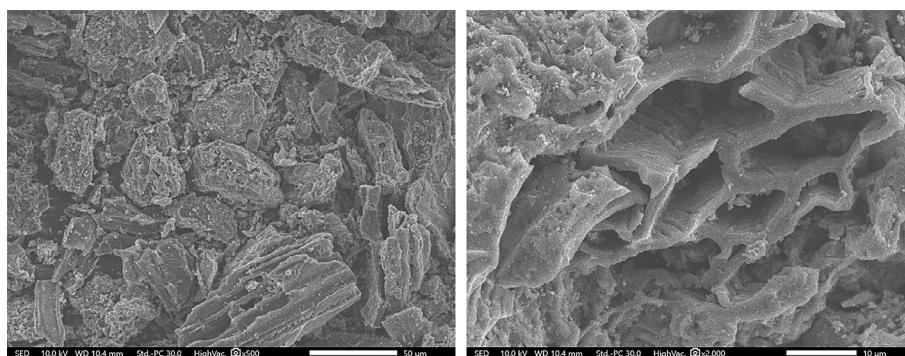
Figure 2. SEM images of FeMn/BC
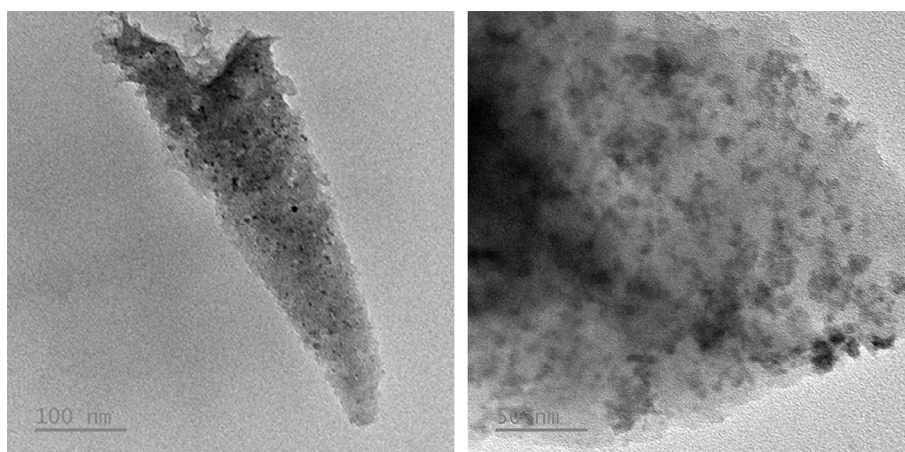
Figure 3. TEM images of FeMn/BC

given scale bars, the particle sizes are estimated to range from approximately 5 to 20 nm. The pronounced contrast between the nanoparticles and the support indicates successful incorporation and homogeneous dispersion of the metal-based nanoparticles within the BC matrix. This nanostructural configuration, featuring high dispersion density and minimal particle agglomeration, is anticipated to enhance the catalytic performance of the FeMn/BC nanocomposite.

The magnetic properties of FeMn/BC were evaluated using VSM at room temperature (Figure 4). Based on the narrow hysteresis loop observed, FeMn/BC could be magnetized and demagnetized easily. Since FeMn/BC contains both Fe^0, Fe_3O_4 and MnO, its magnetism can be attributed to contributions from those components. Pandey et al. (Pandey et al., 2013) assert that MnO demonstrates antiferromagnetic behavior with a negligible M_S. In contrast, Fe^0 and Fe_3O_4 are known to exhibit typical ferromagnetic and ferrimagnetic characteristics, respectively (Nguyen et al., 2021). Hence, the magnetic properties of FeMn/BC mainly come from iron-based crystals. In fact, M_S of FeMn/BC (5.72 wt% Fe) reached 5.13 emu/g, which is comparable to those reported in previous studies for Fe_3O_4/BC: 6.94 emu/g (Do et al., 2022), 7.65 emu/g (Nguyen et al., 2023b), 6.83 emu/g (Nguyen et al., 2023a). These magnetic properties are sufficient to enable efficient
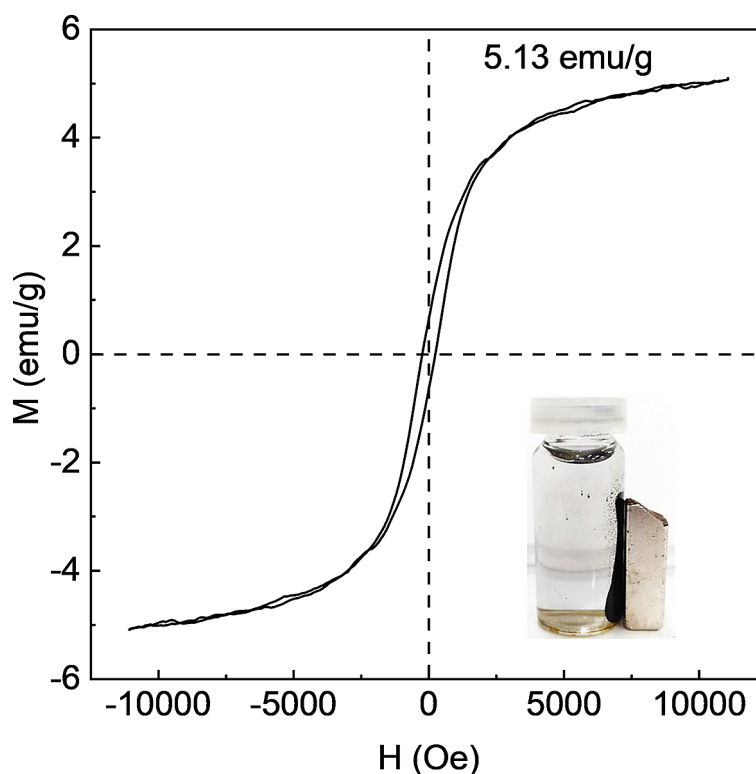
Figure 4. VSM result of FeMn/BC

magnetic separation and recovery of the material after use.

FTIR spectroscopy of FeMn/BC is shown in Figure 5. A broad peak at 3256 cm⁻¹ corresponds to O–H stretching vibrations, indicating the presence of hydroxyl groups, likely from BC or adsorbed water. A peak at 2821 cm⁻¹ is attributed to C–H stretching of aliphatic groups, while the band at 1987 cm⁻¹ likely represents overtones or combination bands of carboxylic or carbonyl groups in BC. A peak at 1522 cm⁻¹ is indicative of C=C aromatic stretching, suggesting aromatic structures within the BC. The strong band at 1116 cm⁻¹ is associated with C–O–C or C–O stretching, pointing to ether or alcohol functionalities. Notably, the peaks at 877 cm⁻¹ and 515 cm⁻¹ correspond to Fe–O and Mn–O vibrations, confirming the presence of metal oxide nanoparticles (Tang et al., 2022). These spectral features indicate that the BC matrix contains various functional groups capable of anchoring or interacting with metal-based nanoparticles, which is beneficial for interaction with water-soluble matter during TZ treatment.

Tartrazine degradation using FeMn/BC

Figure 6 presents TZ degradation using H_2O_2+UV, FeMn/BC+H_2O_2, and FeMn/BC+H_2O_2+UV systems. After 10 min of introducing FeMn/BC, only 4.8% TZ was removed, corresponding to an adsorption capacity of 4.8 mg/g. In the next oxidation step, TZ degradation varied according to treatment conditions. The use of H_2O_2 and UV triggered negligible TZ degradation over an extended period. In the case of FeMn/BC+H_2O_2 system, 63.3% TZ was eliminated after 120 min of oxidation, indicating the catalytic activity of FeMn/BC. With simultaneously additional UV, TZ removal reached 92.0%. These results prove the promising photo-Fenton activity of FeMn/BC.

As seen from Figure 7, BC was not effective in catalyzing H_2O_2 under UV light to eliminate TZ. In contrast, Fe/BC and Mn/BC exhibit moderate catalytic performance, achieving TZ removal of 44.6 and 33.3%, respectively, after 120 min. Remarkably, FeMn/BC demonstrates superior degradation efficiency, removing 92.0% TZ within the same period. This enhanced activity is attributed to the synergistic interaction between Fe and Mn oxides, which promotes efficient generation of reactive hydroxyl
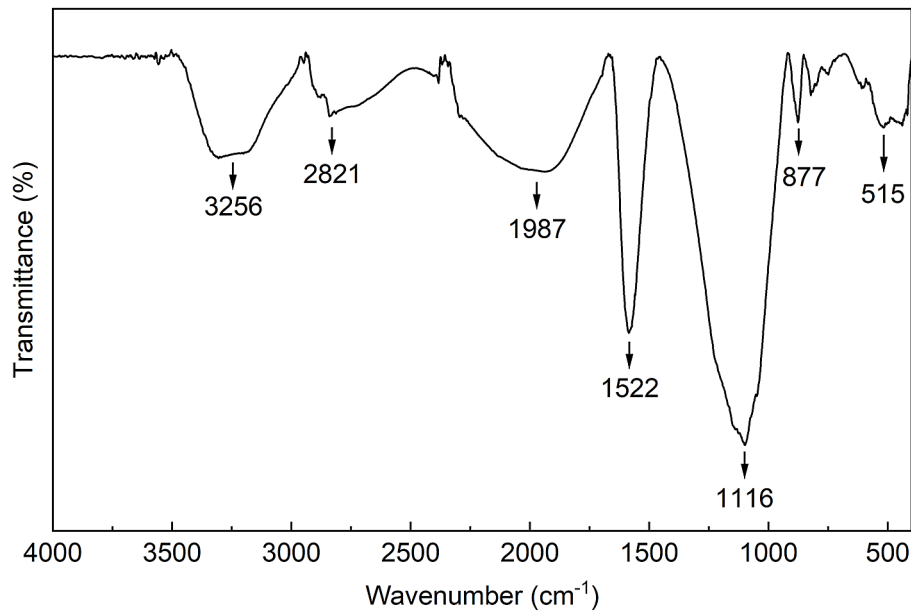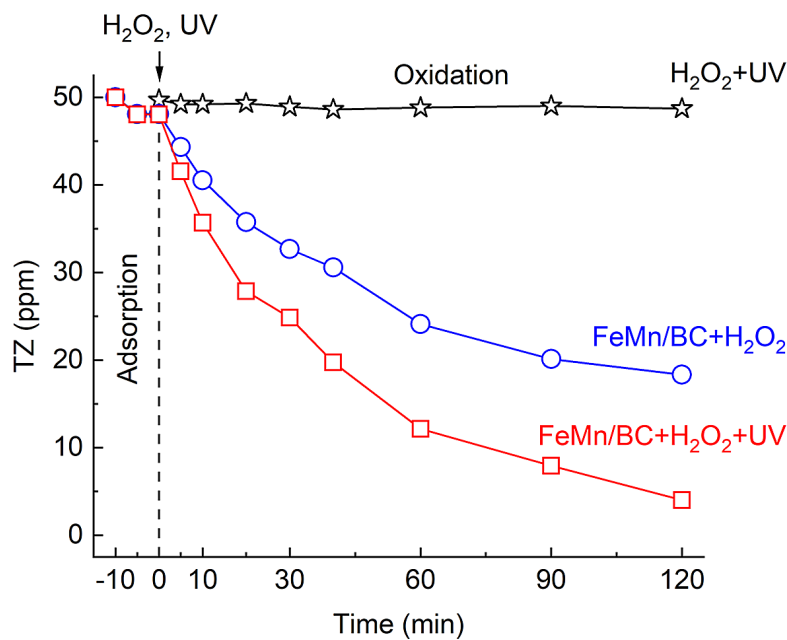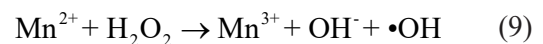
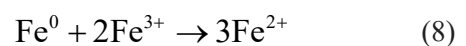**Figure 5.** FTIR spectroscopy of FeMn/BC

Figure 6. TZ degradation by H_2O_2+UV, FeMn/BC+H_2O_2, and FeMn/BC+H_2O_2+
UV systems (0.50 g/L FeMn/BC, 200 ppm H_2O_2, pH 3.0)

radicals under photo-Fenton conditions, thereby accelerating TZ degradation. Based on previous research, catalytic mechanism of FeMn/BC for photo-Fenton degradation of TZ is proposed as follows (Li et al., 2019; Li et al., 2021):
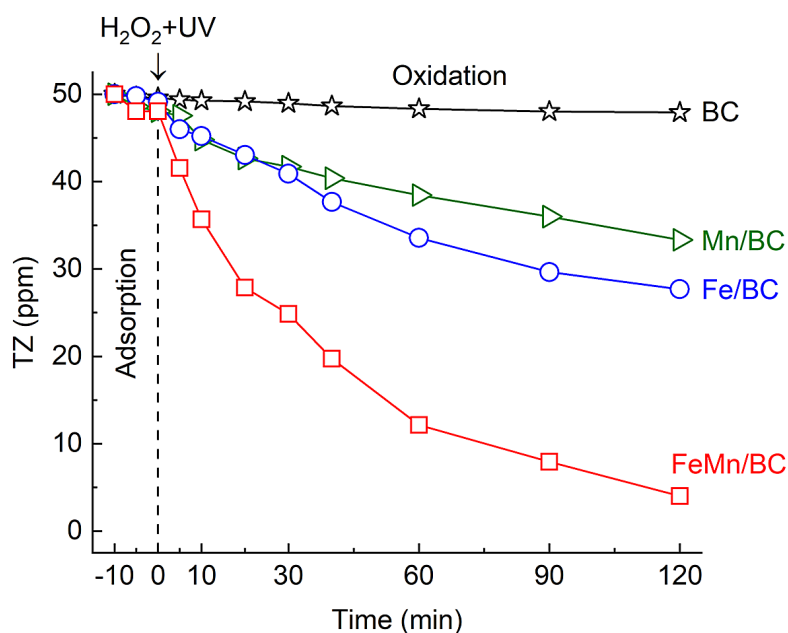
$$Fe^0 + 2H^+ \rightarrow Fe^{2+} + H_2 \quad (3)$$

$$Fe^0 + H_2O_2 + 2H^+ \rightarrow Fe^{2+} + 2H_2O \quad (4)$$

$$Fe^0 + O_2 + 2H^+ \rightarrow Fe^{2+} + H_2O_2 \quad (5)$$

$$Fe^{2+} + H_2O_2 \rightarrow Fe^{3+} + \bullet OH + OH^- \quad (6)$$

$$Fe^{3+} + H_2O_2 \rightarrow Fe^{2+} + + H^+ + \bullet OOH \quad (7)$$

$$Fe^0 + 2Fe^{3+} \rightarrow 3Fe^{2+} \quad (8)$$

$$Mn^{2+} + H_2O_2 \rightarrow Mn^{3+} + OH^- + \bullet OH \quad (9)$$
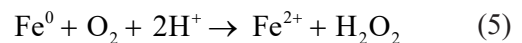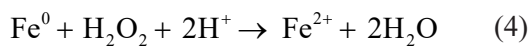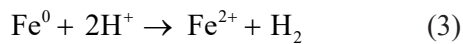
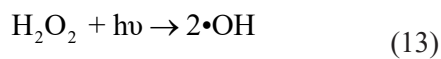**Figure 7.** TZ degradation catalyzed by BC, Fe/BC, Mn/BC and FeMn/BC (0.50 g/L catalyst, 200 ppm H₂O₂, pH 3.0)

$$Mn^{3+} + H_2O_2 \rightarrow Mn^{2+} + \bullet OOH + H^+ \quad (10)$$

$$Mn^{3+} + Fe^{2+} \rightarrow Fe^{3+} + Mn^{2+} \quad (11)$$

$$Fe^{3+} + H_2O + h\upsilon \rightarrow Fe^{2+} + \bullet OH + H^+ \quad (12)$$

$$H_2O_2 + h\upsilon \rightarrow 2\bullet OH \quad (13)$$

$$TZ + \bullet OH \rightarrow Intermediates \rightarrow \rightarrow Mineralization \quad (14)$$
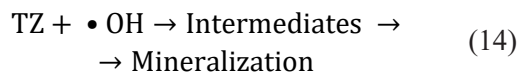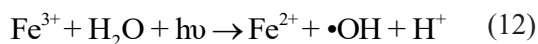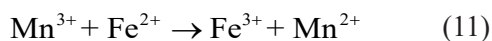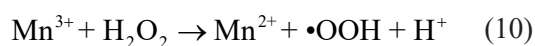
Fe₃O₄ contains both Fe²⁺ and Fe³⁺, while Fe⁰ could be oxidized into Fe²⁺ via different pathways. Fe²⁺ sites could then produce •OH from H₂O₂. Reversely, Fe³⁺ could regenerate Fe²⁺ by H₂O₂ or Fe⁰. In a similar route, the Mn³⁺/Mn²⁺ cycle could also produce •OH. Notably, synergistic interaction between Fe- and Mn-based sites is shown in Equation 11. Additionally, UV light could improve the Fe³⁺/Fe²⁺ cycle and accelerate •OH production (Jiang et al., 2022). Thus, all metal-based materials in
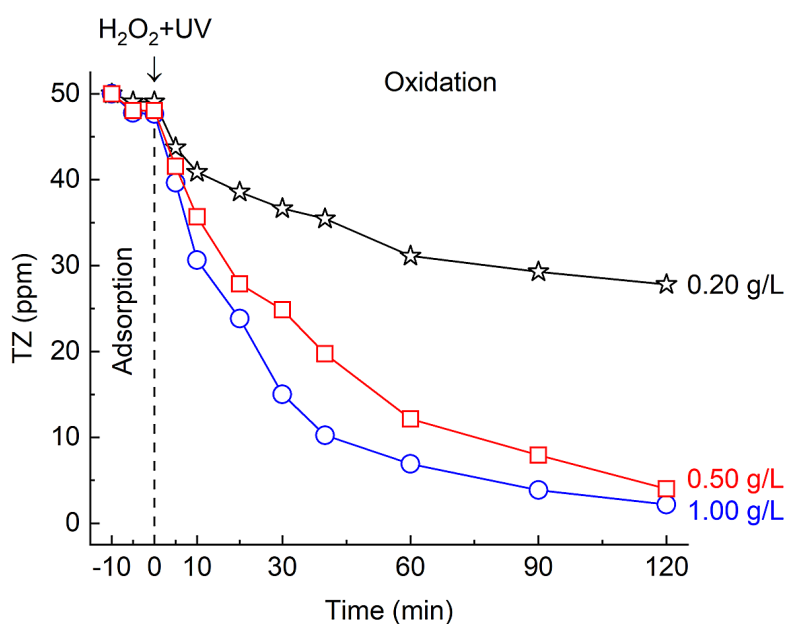

Figure 8. Effect of FeMn/BC dosage on TZ degradation (200 ppm H₂O₂, pH 3.0)
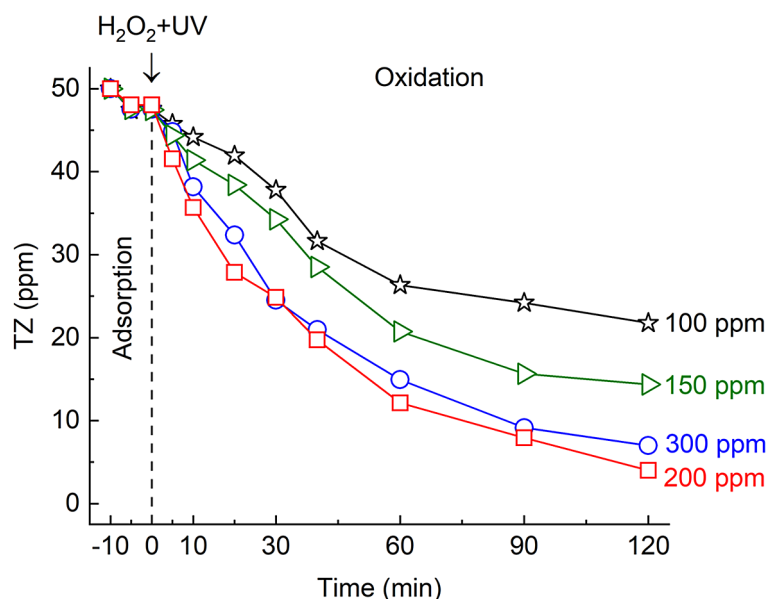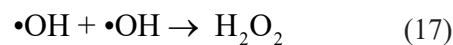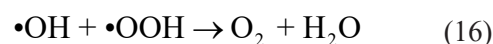
Figure 9. Effect of H₂O₂ concentration on TZ degradation (0.50 g/L FeMn/BC, pH 3.0)

FeMn/BC could potentially contribute to the catalytic photo-Fenton degradation of TZ.

TZ degradation rate was significantly influenced by FeMn/BC dosage (Figure 8). At a lower dosage of 0.20 g/L, the catalyst exhibited limited TZ removal of 44.4% after 120 min. Increasing the FeMn/BC dosage to 0.50 g/L considerably enhanced TZ degradation. This enhancement can be attributed to the increased availability of active sites, which facilitate more generation of free radicals. Nevertheless, a further increase to 1.00 g/L slightly improved TZ degradation rate. This marginal gain suggests that an excess of active sites may lead to non-productive consumption of •OH radicals, thereby reducing their availability for attacking TZ molecules. Thus, while increasing catalyst dosage enhances degradation up to a certain point, excessively high concentrations may lead to reduced efficiency due to radical scavenging.

As depicted in Figure 9, increasing the H₂O₂ concentration from 100 to 200 ppm significantly enhanced TZ removal, with efficiency rising from 56.4% to a peak of 92.0%. This improvement is attributed to the greater generation of •OH for TZ degradation. However, when the H₂O₂ concentration is further increased to 300 ppm, TZ removal slightly dropped to 86.0%. This decline is likely due to scavenging reactions, which diminish available •OH radicals (Equations 15–17) (Youssef et al., 2016).

$$\bullet OH + H_2O_2 \rightarrow \bullet OOH + H_2O \quad (15)$$

$$\bullet OH + \bullet OOH \rightarrow O_2 + H_2O \quad (16)$$

$$\bullet OH + \bullet OH \rightarrow H_2O_2 \quad (17)$$

CONCLUSIONS

In this study, FeMn/BC was prepared via one-pot pyrolysis using durian husks, KMnO₄, and FeCl₃. XRD and ICP analyses confirmed that FeMn/BC consisted of 5.72 wt% Fe (Fe₃O₄ and Fe⁰) and 2.90 wt% Mn (MnO). TEM images revealed that metal-based nanoparticles were well dispersed within the BC matrix. In addition, FeMn/BC had S_{BET} of 292 m²/g and V_{total} of 0.19 cm³/g. Accordingly, the catalytic activity of FeMn/BC was investigated for photo-Fenton degradation of TZ. At pH 3.0, 50 ppm TZ, 200 ppm H₂O₂, and 0.50 g/L FeMn/BC, TZ removal of 92.0% was achieved after 10 min of adsorption and 120 min of UV-assisted oxidation. Additionally, FeMn/BC showed magnetic properties with a M_S of 5.13 emu/g, enabling easy recovery using a magnet. These findings highlight the multifunctional nature and practical potential of FeMn/BC for the effective treatment of dye-contaminated wastewater.

REFERENCES

1. Ahmed, Y., Maya, A. A. S., Akhtar, P., AlMohamadi, H., Mohammad, A. W., Ashekuzzaman, S. M., Olbert, A. I., Uddin, M. G. (2025). Advancements and challenges in Fenton-based advanced oxidation processes for antibiotic removal in wastewater: From the laboratory to practical applications. *Journal of Environmental Chemical Engineering*, *13*(1), 115068. https://doi.org/10.1016/j.jece.2024.115068

2. Amchova, P., Siska, F., Ruda-Kucerova, J. (2024). Safety of tartrazine in the food industry and potential protective factors. *Heliyon*, *10*(18), e38111. https://doi.org/10.1016/j.heliyon.2024.e38111

3. Bedia, J., Peñas-Garzón, M., Gómez-Avilés, A., Rodriguez, J. J., Belver, C. (2020). Review on activated carbons by chemical activation with $FeCl_3$. *C*, *6*(2), 21. https://doi.org/10.3390/c6020021

4. Brillas, E. (2022). Fenton, photo-Fenton, electro-Fenton, and their combined treatments for the removal of insecticides from waters and soils. A review. *Separation and Purification Technology*, *284*, 120290. https://doi.org/10.1016/j.seppur.2021.120290

5. Brillas, E., Garcia-Segura, S. (2020). Benchmarking recent advances and innovative technology approaches of Fenton, photo-Fenton, electro-Fenton, and related processes: A review on the relevance of phenol as model molecule. *Separation and Purification Technology*, *237*, 116337. https://doi.org/10.1016/j.seppur.2019.116337

6. Cao, J., Li, J., Yang, B., Chen, Z., Mahjoub, A. R., Xing, M. (2024). Gambling of homogeneous and heterogeneous Fenton in wastewater treatment. *Cell Reports Physical Science*, *5*(5), 101966. https://doi.org/10.1016/j.xcrp.2024.101966

7. Chang, F., Li, H. (2024). Preparation of high-efficient $KMnO_4$ modified biochar for heavy metal removal from municipal wastewater. *Arabian Journal of Chemistry*, *17*(5), 105756. https://doi.org/10.1016/j.arabjc.2024.105756

8. Chen, Z., Zheng, Y., Liu, Y., Zhang, W., Wang, Y., Guo, X., Tang, X., Zhang, Y., Wang, Z., Zhang, T. (2019). Magnetic Mn-doped Fe_3O_4 hollow microsphere/RGO heterogeneous photo-Fenton catalyst for high efficiency degradation of organic pollutant at neutral pH. *Materials Chemistry and Physics*, *238*, 121893. https://doi.org/10.1016/j.matchemphys.2019.121893

9. Do, T. V. T., Bui, Q. L. N., Nguyen, H. M., Lam, H. H., Tran-Thuy, T.-M., Nguyen, L. Q., Ngo, D. T. H., Nguyen, D. V. (2022). One-pot fabrication of magnetic biochar by $FeCl_3$-activation of lotus seed-pod and its catalytic activity towards degradation of Orange G. *Materials Research Express*, *9*(10), 105601. https://doi.org/10.1088/2053-1591/ac9819

10. Faheem, Du, J., Kim, S. H., Hassan, M. A., Irshad, S., Bao, J. (2020). Application of biochar in advanced oxidation processes: supportive, adsorptive, and catalytic role. *Environmental Science and Pollution Research*, *27*(30), 37286-37312. https://doi.org/10.1007/s11356-020-07612-y

11. Hardyanti, N., Zaman, B., Anisa Pramesti, I., Stanley William, G., Purwono, P. (2024). Integrated ozone-Fenton treatment – A breakthrough in pharmaceutical wastewater purification. *Ecological Engineering & Environmental Technology*, *25*(11), 228–240. https://doi.org/10.12912/27197050/192607

12. Hussain, S., Aneggi, E., Goi, D. (2021). Catalytic activity of metals in heterogeneous Fenton-like oxidation of wastewater contaminants: a review. *Environmental Chemistry Letters*, *19*(3), 2405–2424. https://doi.org/10.1007/s10311-021-01185-z

13. Intisar, A., Ramzan, A., Hafeez, S., Hussain, N., Irfan, M., Shakeel, N., Gill, K. A., Iqbal, A., Janczarek, M., Jesionowski, T. (2023). Adsorptive and photocatalytic degradation potential of porous polymeric materials for removal of pesticides, pharmaceuticals, and dyes-based emerging contaminants from water. *Chemosphere*, *336*, 139203. https://doi.org/10.1016/j.chemosphere.2023.139203

14. Jamnongkan, T., Intaramongkol, N., Kanjanaphong, N., Ponjaroen, K., Sriwiset, W., Mongkholrattanasit, R., Wongwachirakorn, P., Lin, K.-Y. A., Huang, C.-F. (2022). Study of the enhancements of porous structures of activated carbons produced from durian husk wastes. *Sustainability*, *14*(10), 5896. https://doi.org/10.3390/su14105896

15. Jiang, Y., Ran, J., Mao, K., Yang, X., Zhong, L., Yang, C., Feng, X., Zhang, H. (2022). Recent progress in Fenton/Fenton-like reactions for the removal of antibiotics in aqueous environments. *Ecotoxicology and Environmental Safety*, *236*, 113464. https://doi.org/10.1016/j.ecoenv.2022.113464

16. Lee, M. C., Koay, S. C., Chan, M. Y., Choo, H. L., Pang, M. M., Chou, P. M., Tshai, K. Y. (2019). Properties of poly(lactic acid)/durian husk fiber biocomposites: Effects of fiber content and processing aid. *Journal of Thermoplastic Composite Materials*, *33*(11), 1518-1532. https://doi.org/10.1177/0892705719831734

17. Li, L., Lai, C., Huang, F., Cheng, M., Zeng, G., Huang, D., Li, B., Liu, S., Zhang, M., Qin, L., Li,

M., He, J., Zhang, Y., Chen, L. (2019). Degradation of naphthalene with magnetic bio-char activate hydrogen peroxide: Synergism of bio-char and Fe–Mn binary oxides. *Water Research*, *160*, 238-248. https://doi.org/10.1016/j.watres.2019.05.081

18. Li, L., Liu, S., Cheng, M., Lai, C., Zeng, G., Qin, L., Liu, X., Li, B., Zhang, W., Yi, Y., Zhang, M., Fu, Y., Li, M., Long, M. (2021). Improving the Fenton-like catalytic performance of MnO_x-Fe_3O_4/biochar using reducing agents: A comparative study. *Journal of Hazardous Materials*, *406*, 124333. https://doi.org/10.1016/j.jhazmat.2020.124333

19. Li, X., Shen, X., Jiang, W., Xi, Y., Li, S. (2024). Comprehensive review of emerging contaminants: Detection technologies, environmental impact, and management strategies. *Ecotoxicology and Environmental Safety*, *278*, 116420. https://doi.org/10.1016/j.ecoenv.2024.116420

20. Liu, Y., Wang, J. (2023). Multivalent metal catalysts in Fenton/Fenton-like oxidation system: A critical review. *Chemical Engineering Journal*, *466*, 143147. https://doi.org/10.1016/j.cej.2023.143147

21. Mekuye, B., Abera, B. (2023). Nanomaterials: An overview of synthesis, classification, characterization, and applications. *Nano Select*, *4*(8), 486–501. https://doi.org/10.1002/nano.202300038

22. Mohd Ali, M., Hashim, N., Aziz, S. A., Lasekan, O. (2020). Exploring the chemical composition, emerging applications, potential uses, and health benefits of durian: A review. *Food Control*, *113*, 107189. https://doi.org/10.1016/j.foodcont.2020.107189

23. Nguyen, H. M., Truong, T. B., Nguyen, H.-H. T., Tran, P. T., Tran-Thuy, T.-M., Nguyen, L. Q., Nguyen, D. V. (2023a). Catalytic ozonation of Ponceau 4R using multifunctional magnetic biochar prepared from rubber seed shell. *Journal of Ecological Engineering*, *24*(12), 143–151. https://doi.org/10.12911/22998993/172919

24. Nguyen, L. T. K., Nguyen, L. Q., Nguyen, H. M., Nguyen, T. M., Lam, H. H., Tran-Thuy, T.-M., Nguyen, D. V. (2023b). Simple one-step synthesis of nipa frond-derived magnetic porous carbon for decolorization of acid yellow 23. *Journal of Chemistry*, *2023*, 5447693. https://doi.org/10.1155/2023/5447693

25. Nguyen, M. D., Tran, H.-V., Xu, S., Lee, T. R. (2021). Fe_3O_4 nanoparticles: Structures, synthesis, magnetic properties, surface functionalization, and emerging applications. *Applied Sciences*, *11*(23), 11301. https://doi.org/10.3390/app112311301

26. Nguyen, N. T. K., Le, D. T. T., Vo, K. D., Huynh, L. T., Nguyen, H. M., Tran-Thuy, T.-M., Nguyen, L. Q., Nguyen, D. V. (2024a). Valorization of tropical almond (*Terminalia catappa*) leaves into iron-containing activated carbon for rapid catalytic degradation of methylene blue with hydrogen peroxide [journal article]. *Journal of Ecological Engineering*, *25*(8), 54–61. https://doi.org/10.12911/22998993/189672

27. Nguyen, N. T. H., Nguyen, T. T. T., Nguyen, D. T. C., Tran, T. V. (2024b). A comprehensive review on the production of durian fruit waste-derived bioadsorbents for water treatment. *Chemosphere*, *363*, 142801. https://doi.org/10.1016/j.chemosphere.2024.142801

28. O'Dowd, K., Pillai, S. C. (2020). Photo-Fenton disinfection at near neutral pH: Process, parameter optimization and recent advances. *Journal of Environmental Chemical Engineering*, *8*(5), 104063. https://doi.org/10.1016/j.jece.2020.104063

29. Pandey, B. K., Shahi, A. K., Gopal, R. (2013). Synthesis, optical properties and growth mechanism of MnO nano structures. *Applied Surface Science*, *283*, 430–437. https://doi.org/10.1016/j.apsusc.2013.06.126

30. Qiu, D., Guo, N., Gao, A., Zheng, L., Xu, W., Li, M., Wang, F., Yang, R. (2019). Preparation of oxygen-enriched hierarchically porous carbon by $KMnO_4$ one-pot oxidation and activation: Mechanism and capacitive energy storage. *Electrochimica Acta*, *294*, 398–405. https://doi.org/10.1016/j.electacta.2018.10.049

31. Rahim Pouran, S., Abdul Aziz, A. R., Wan Daud, W. M. A. (2015). Review on the main advances in photo-Fenton oxidation system for recalcitrant wastewaters. *Journal of Industrial and Engineering Chemistry*, *21*, 53–69. https://doi.org/10.1016/j.jiec.2014.05.005

32. Ribeiro, J. P., Gomes, H. G. M. F., Sarinho, L., Marques, C. C., Nunes, M. I. (2022). Synergies of metallic catalysts in the Fenton and photo-Fenton processes applied to the treatment of pulp bleaching wastewater. *Chemical Engineering and Processing - Process Intensification*, *181*, 109159. https://doi.org/10.1016/j.cep.2022.109159

33. Shrestha, S., Wang, B., Dutta, P. (2020). Nanoparticle processing: Understanding and controlling aggregation. *Advances in Colloid and Interface Science*, *279*, 102162. https://doi.org/10.1016/j.cis.2020.102162

34. Soffian, M. S., Abdul Halim, F. Z., Aziz, F., A. Rahman, M., Mohamed Amin, M. A., Awang Chee, D. N. (2022). Carbon-based material derived from biomass waste for wastewater treatment. *Environmental Advances*, *9*, 100259. https://doi.org/10.1016/j.envadv.2022.100259

35. Tang, S.-F., Zhou, H., Tan, W.-T., Huang, J.-G., Zeng, P., Gu, J.-F., Liao, B.-H. (2022). Adsorption characteristics and mechanisms of Fe-Mn oxide modified biochar for Pb(II) in wastewater. *International Journal of Environmental Research and Public Health*, *19*(14), 8420. https://doi.org/10.3390/ijerph19148420

36. Tran, P. T., Nguyen, H. M., Vo, K. D., Nguyen, L. Q.,

Tran-Thuy, T.-M., Nguyen, D. V. (2024a). Simple preparation of iron oxide-loaded biochar from *Ceratophyllum demersum* for Fenton-like degradation of Rhodamine B. *Ecological Engineering & Environmental Technology*, *25*(10), 297–305. https://doi.org/10.12912/27197050/191989

37. Tran, T. T. C., Phan, A. T. N., Nguyen, H. M., Nguyen, L. Q., Tran-Thuy, T.-M., Le, T. X., Nguyen, D. V. (2024b). Simple fabrication of copper nanoparticle-loaded biochar from rosemary extraction residues for peroxydisulfate activation towards Ponceau 4R decolorization. *Journal of Ecological Engineering*, *25*(10), 136–145. https://doi.org/10.12911/22998993/191950

38. Wen, Y., Schoups, G., van de Giesen, N. (2017). Organic pollution of rivers: Combined threats of urbanization, livestock farming and global climate change. *Scientific Reports*, *7*(1), 43289. https://doi.org/10.1038/srep43289

39. Youssef, N. A., Shaban, S. A., Ibrahim, F. A., Mahmoud, A. S. (2016). Degradation of methyl orange using Fenton catalytic reaction. *Egyptian Journal of Petroleum*, *25*(3), 317–321. https://doi.org/10.1016/j.ejpe.2015.07.017

40. Yuan, X., Cao, Y., Li, J., Patel, A. K., Dong, C.-D., Jin, X., Gu, C., Yip, A. C. K., Tsang, D. C. W., Ok, Y. S. (2023). Recent advancements and challenges in emerging applications of biochar-based catalysts. *Biotechnology Advances*, *67*, 108181. https://doi.org/10.1016/j.biotechadv.2023.108181

41. Zhang, M.-h., Dong, H., Zhao, L., Wang, D.-x., Meng, D. (2019). A review on Fenton process for organic wastewater treatment based on optimization perspective. *Science of The Total Environment*, *670*, 110–121. https://doi.org/10.1016/j.scitotenv.2019.03.180

42. Zheng, J., Lim, H. J., Hedtke, T., Kim, J.-H., Zhang, S. (2024). Manganese oxide for heterogeneous Fenton treatment: Catalyst or inhibitor? *Applied Catalysis B: Environment and Energy*, *359*, 124531. https://doi.org/10.1016/j.apcatb.2024.124531

43. Zhu, Q.-L., Xu, Q. (2016). Immobilization of ultrafine metal nanoparticles to high-surface-area materials and their catalytic applications. *Chem*, *1*(2), 220–245. https://doi.org/10.1016/j.chempr.2016.07.005

44. Zhu, Y., Zhu, R., Xi, Y., Zhu, J., Zhu, G., He, H. (2019). Strategies for enhancing the heterogeneous Fenton catalytic reactivity: A review. *Applied Catalysis B: Environmental*, *255*, 117739. https://doi.org/10.1016/j.apcatb.2019.05.041

45. Ziembowicz, S., Kida, M. (2022). Limitations and future directions of application of the Fenton-like process in micropollutants degradation in water and wastewater treatment: A critical review. *Chemosphere*, *296*, 134041. https://doi.org/10.1016/j.chemosphere.2022.134041